JMES The International Journal of Mechanical Engineering and Sciences
https://iptek.its.ac.id/index.php/jmes
e-ISSN 2580-7471

# Static Load Analysis of Rectangular and I-Wing Spar Profiles: A Comparative Study between Mathematical and Finite Element Methods

Widyawasta[1,2*], Alief Wikarta[2]
[1]National Research and Innovation Agency, Jakarta, Indonesia
[2]Department of Mechanical Engineering, ITS, Sukolilo Surabaya 60111, Indonesia

*Received: 12 February 2024, Revised: 19 February 2024, Accepted: 21 February 2024*

**Abstract**

Unmanned aerial vehicles (UAVs) have become increasingly essential in both civilian and military contexts, serving various roles such as surveillance, mapping, cargo transport, and specialized tasks. The demand for long-endurance surveillance UAVs is critical for covering vast areas continuously, prompting the development of Medium Altitude Long Endurance (MALE UAV). This paper explores the structural strength analysis of various wing spar profiles of MALE UAVs using mathematical analysis and Finite Element Method (FEM) under static loads. The wings, pivotal for generating lift, are subjected to rigorous operational loads, necessitating robust structural reliability. While mathematical analysis provides fundamental insights, FEM allows for detailed simulations under various conditions. Comparative studies between mathematical analysis and FEM are conducted to validate the structural strength of MALE UAV wings, with a focus on different spar profiles. Aluminum Al7075-T6 is used as the material, with convergence tests ensuring FEM accuracy. The comparative analysis highlights significant variations in normal and shear stress among different spar profiles, with the widest disparities observed at the wing root, 8.76 and 12.04 MPa resp., and the least, 2.87 and 2.87 MPa, close to the wing tip position at 6.75 m. These insights underscore the critical role of structural integrity in optimizing UAV performance and reliability.

**Keywords: structural strength, FEM, spar profiles, mathematical analysis**

## 1. Introduction

The role of unmanned aerial vehicles (UAVs) has been increasingly prominent recently, both for civilian and military purposes, serving as surveillance aircraft, mapping tools, cargo transporters, and flying robots for various specialized tasks [1] [2]. The author's institution has developed various types of fixed-wing UAVs, including the compact tailless model's "Sriti" [3], and surveillance drones deployable from sea vessels. Furthermore, there is the larger "Wulung" UAV [4], weighing 120 kg and capable of covering a range of 200 km. This aircraft serves functional purposes, such as carrying flares for artificial rain cloud seeding. The demand for long-endurance surveillance UAVs is critical to reaching vast and continuous areas. Therefore, the initiative to develop Medium Altitude Long Endurance (MALE) UAVs is underway.

The capability for extended flight duration not only requires a high volume and efficient fuel consumption but also demands strong structural reliability to endure operational loads, primarily borne by the wings.

Wings are the primary aircraft components generating lift force. The wing structure comprises various sections, as depicted in Figure 1, with the spar serving as the main component supporting nearly all the flight loads. The structural configuration of the spar can be observed in Figure 2.

Structural strength analysis of the wing is a crucial aspect of UAV design development. Two common approaches used to analyze structural strength are mathematical analysis and Finite Element Method (FEM). Mathematical analysis, employing theoretical approaches and analytical calculations, provides profound insight into structural behavior at a fundamental level [5]. However, this approach often has limitations in dealing with complex structures and may not precisely model detailed complexities.

On the other hand, FEM is a numerical approach enabling detailed and accurate simulation of UAV [6] wing structural responses to various loads and operational conditions. By discretizing the structure into small elements and applying fundamental physical principles, this method can offer deeper insights into structural behavior at more complex levels [7]. To achieve this objective, the ANSYS finite element analysis software was utilized to develop models featuring varied cross-sectional shapes.

*Corresponding author. Email: widyawasta@brin.go.id.

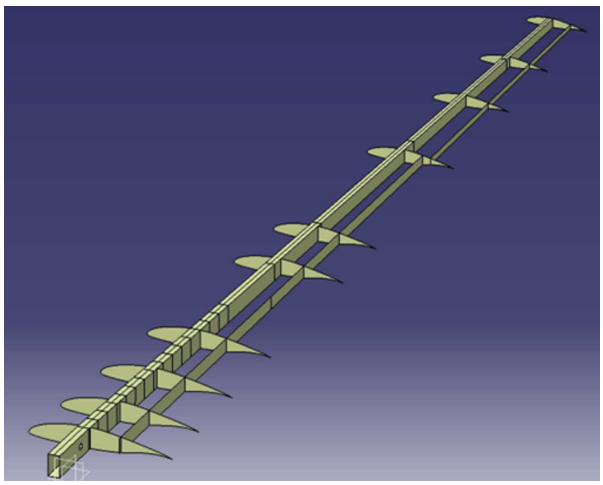

**Figure 1.** Structural Component of Wing

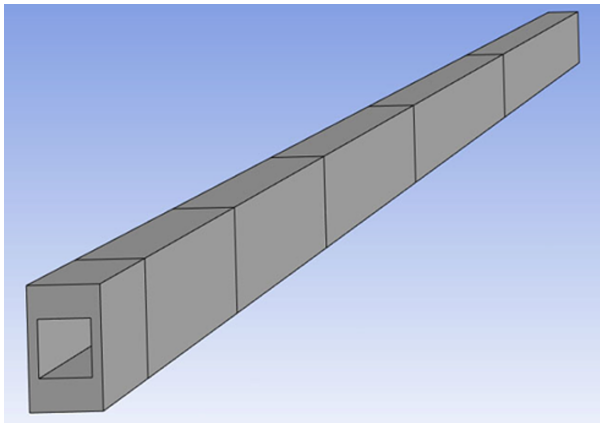

**Figure 2.** Wing Spar

In this paper, a comparative exploration between mathematical analysis and FEM concerning the structural strength of MALE UAV wings will be conducted for validation purposes. Furthermore, a comparison of different profiles used in UAV spar construction will be presented, examining the normal stress and shear stress occurring within the spar.

## 2. Theoretical Method

The object of the study was a MALE UAV which has a capability of 24 hours surveillance with specifications as outlined in Table 1.

For proper aerodynamic and structural analysis of aircraft, it is imperative to accurately determine the distribution of lift force along the wingspan. This distribution can be derived from Prandtl Line theory [8], which is based on the Potential Lift Theory, stating that wing lift can be modeled using potential fluid flow equations. The elliptical lift distribution [9] represents one of the theoretical models of lift force generation. Figure 3 demonstrates this distribution, showing the highest lift concentration in the middle of the wing, tapering off towards its edges.

The aircraft's weight planning is 1,300 kg, and the occurring load factor is limited to 4g. According to FAR 23.302 regulations, the wing structure's strength must have a factor of safety of 1.5, resulting in a total load of 76,518 N.

Since the wing and the lift force acting upon it are symmetrical, calculations need only be performed for half of the wing. Lift force prediction in this preliminary design phase is accomplished using the Schrenk Approximation [10], where the distributed force is divided into several forces acting on each section of the spar. Figure 4 illustrates the division of the spar spanwise with the applied forces.

$$V_{(X)} = \int_x^l L'_{(X)} dx \tag{1}$$

Where,

L = Load applied
x = Position of force

The shear force depicted in Figure 5 shows that the highest force, measuring 37.7 kN, is experienced at the spar root. This force gradually diminishes along the spar with each lift force until it reaches the tip.

Bending moment is derived by the equation,

$$M_{(X)} = \int_x^l V_{(X)} dx \tag{2}$$

Figure 6 demonstrates the bending moment occurring in the spar. The greatest moment is observed at the spar base, totaling 127.38 kNm, and diminishes in a linear fashion with each subsequent force until it vanishes at the spar's tip.

Each spar, which has cross-sectional geometries that are both rectangular and I-profile, has its stress determined for it.

Normal stress is calculated by the formula,

$$\sigma = \frac{M_y}{I_x} dx \tag{3}$$

Where,

$$I_x = \int y^2 dA \tag{4}$$

is the second moment of area of the cross section.

y = Height of the cross section
A = Area of the cross-section shape

**Table 1.** MALE UAV Specification

| | | | |
|---|---|---|---|
| Mass, *W* | : | 1.300.00 | kg |
| Wing span, *b* | : | 16.00 | m |
| Wing Area, *S* | : | 12.80 | $m^2$ |
| Aspect Ratio, *A* | : | 20.00 | |
| Mean Aerodynamic Chord, *MAC* | : | 0.40 | |
| Airspeed, *V* | : | 370.00 | kph |
| Load factor, *n* | : | 4.0 | |
| Factor of safety | : | 1.5 | |

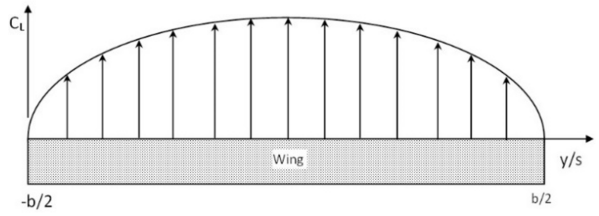


**Figure 3.** A Common Lift Distribution in MALE UAV

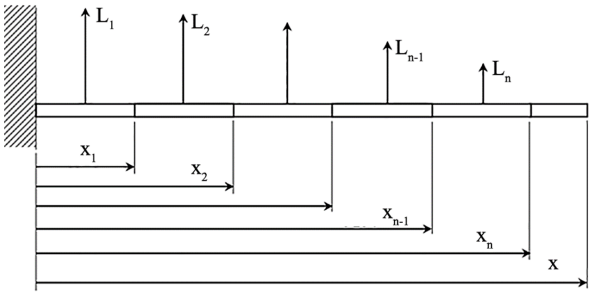


**Figure 4.** Spar Segmentation

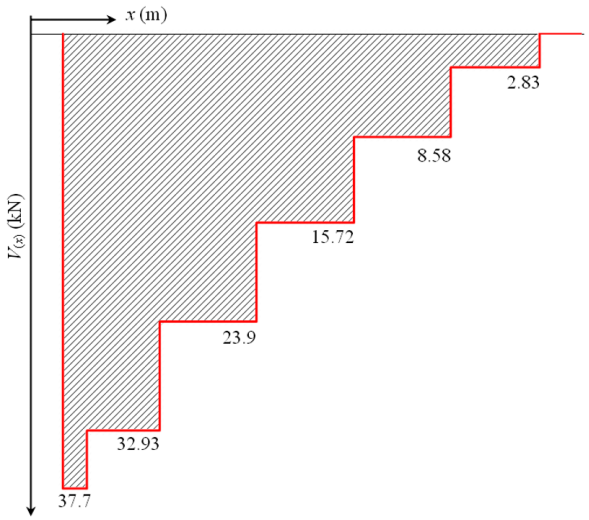


**Figure 5.** Shear Force

Shear stress is obtained by the formula,

$$\tau = \frac{F}{A} \tag{5}$$

where F = applied force

The FEM analysis modeling is performed utilizing ANSYS Discovery. The model encompasses two distinct cross-sectional shapes: rectangular and I-profile. The subsequent procedures are carried out using ANSYS Mechanical, encompassing boundary and load conditions, as depicted in Figure 7. These procedures adhere to the phases of the Schrenk Approximation method, where lift force is applied to each spar segment, and remote displacement is applied at the root of the spar.

The material utilized in this research is Aluminum Al7075-T6, widely employed in aerospace structures [11] due to its lightweight and robust properties. This material exhibits mechanical properties [12] as outlined in Table 2.

The subsequent stage involves meshing, during which the physical domain is partitioned into smaller, finite elements. These elements form a mesh, comprising triangles or quadrilaterals in two dimensions and tetrahedra or hexahedra in three dimensions, to approximate the behavior of the structure or system.

Convergence tests are carried out to ensure that the FEM calculation provides fairly accurate values using appropriate elements.

A convergence test was conducted for each spar profile. Figure 8 indicates that the rectangular spar begins to converge at 150,000 elements sized at 12.5 mm, while the I-profile converges at 100,000 elements with a size of 15 mm. Therefore, these element sizes will be used in the subsequent FEM calculations.

A comparison of the mathematical and FEM calculation results for the rectangular spar at several positions is presented in Table 3. Normal stress on rectangular spar at different locations. Differences in normal stress are observed at the wing root and mid-wing positions.

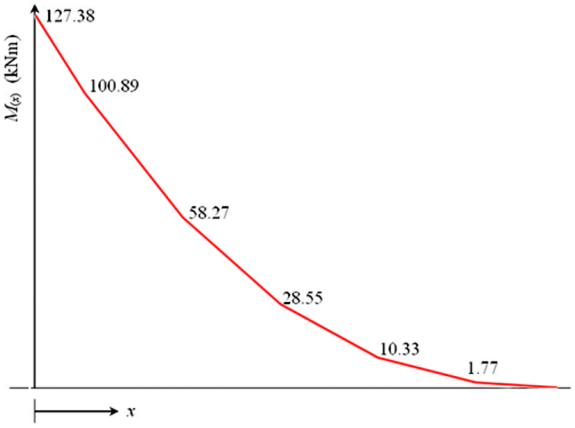


**Figure 6.** Bending Moment

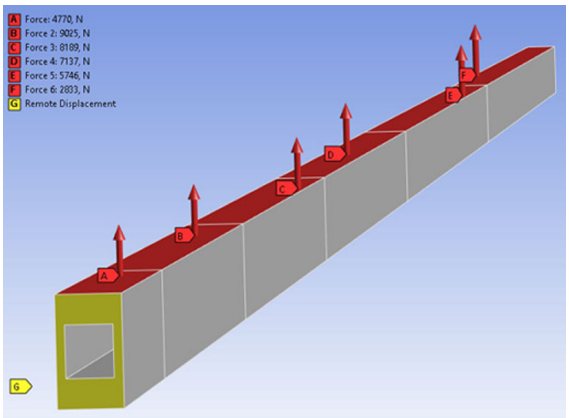


**Figure 7.** Boundary and Loads Condition on FEM

**Table 2.** Mechanical Properties of AI7075-T6

| | |
|---|---|
| Modulus of Elasticity | 71.7 GPa |
| Shear Modulus | 26.9 GPa |
| Tensile Yield Strength | 503 MPa |
| Shear Strength | 331 MPa |
| Poisson's Ratio | 0.33 |
| Density | 2,810 kg/m$^3$ |

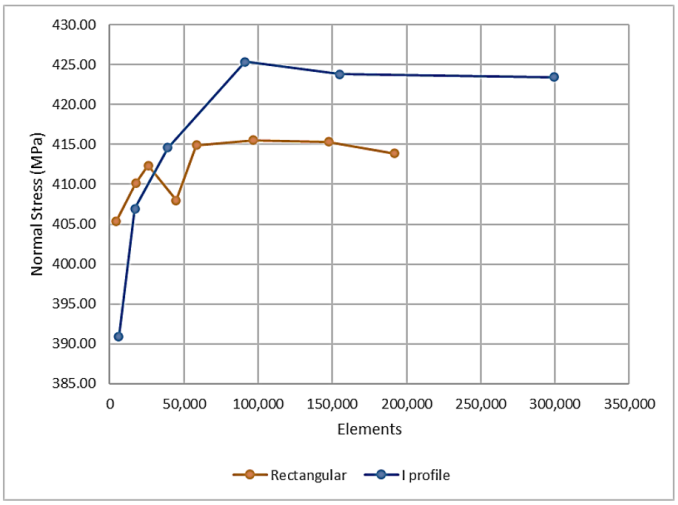


**Figure 8.** Convergence Test for Profiled Spars

**Table 3.** Normal Stress on Rectangular Spar at Different Location

| | Mathematical (MPa) | FEM (MPa) | Difference (%) |
|---|---|---|---|
| Normal Stress (x=0 m) | 421.44 | 415.04 | 1.52 |
| Shear Stress (x=0 m) | 10.47 | 11.47 | 9.57 |
| Normal Stress (x=3.75 m) | 255.17 | 333.37 | 1.93 |
| Shear Stress (x=3.75 m) | 7.07 | 7.03 | 13.64 |

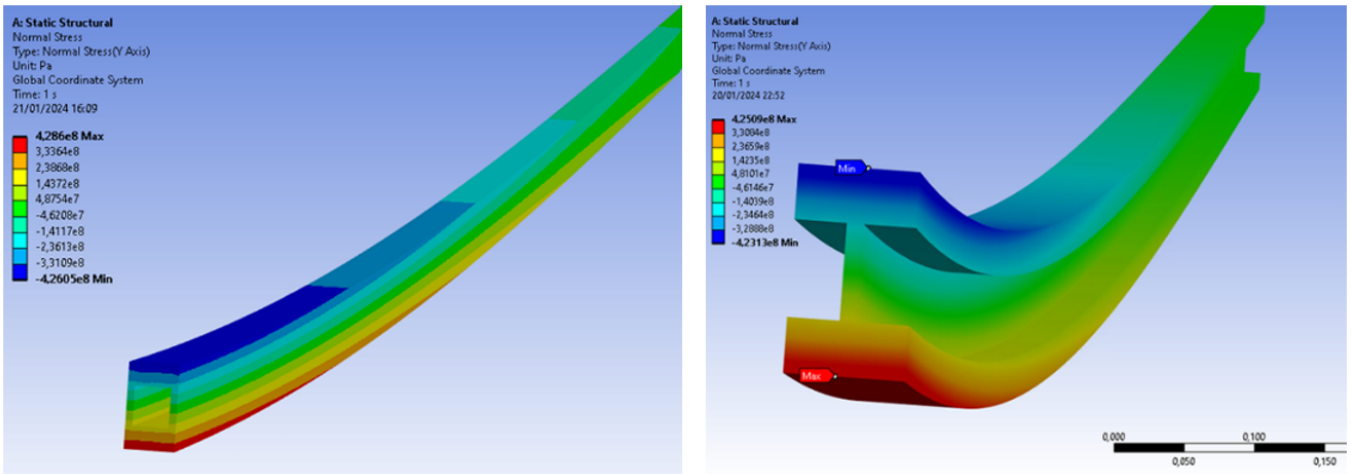


**Figure 9.** Normal Stress on Spar

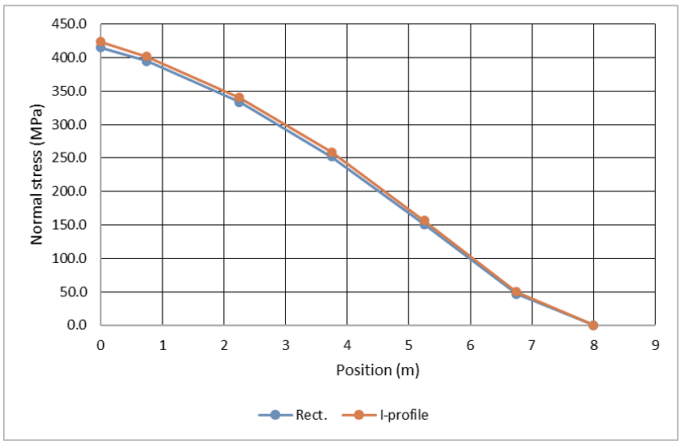


**Figure 10.** Normal Stress Comparison of Different Cross Section

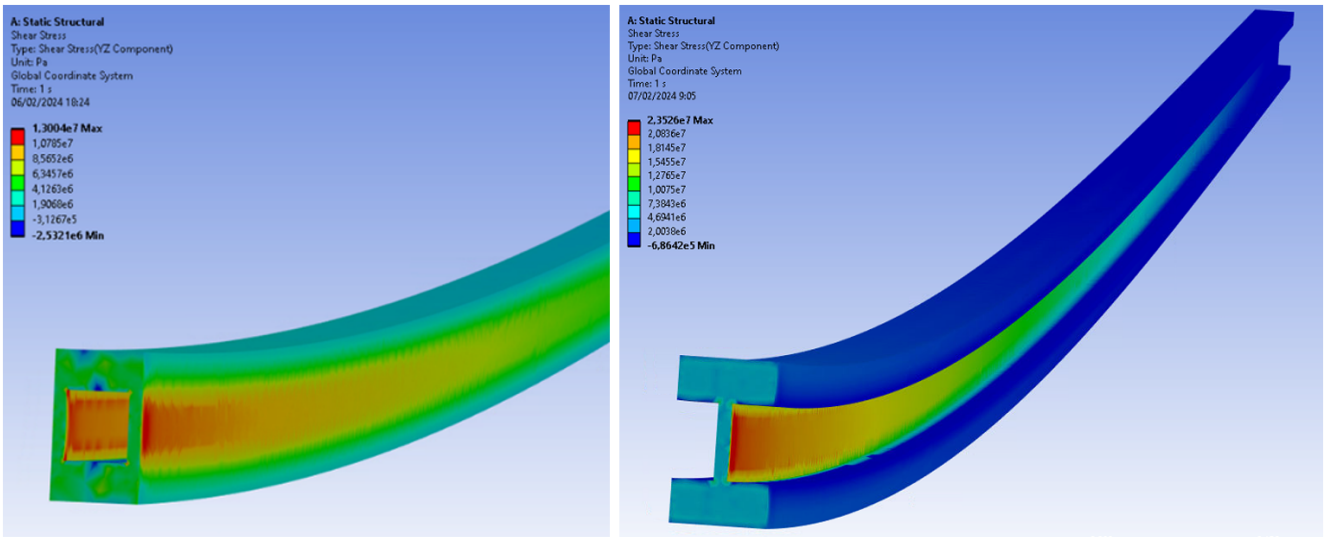


**Figure 11.** Shear Stress on Spar

## 3. Results and Discussion

The FEM analysis findings depicted in Figure 9 reveal the presence of normal stress on both the upper and lower flanges of the spar beam. Under the influence of an upward bending moment, tensile stress develops along the lower section, highlighted in red, while compression manifests in the upper section, depicted in blue and indicated by negative signs. Both profiles exhibit a consistent pattern of normal stress. The highest values are observed on surfaces closer to the root, indicating a proportional increase.

Upon meticulous scrutiny and comparison, it emerges that the normal stress magnitudes observed in both profiled spars exhibit a remarkable degree of similarity, as shown in Figure 10. Specifically, at the root, the normal stress is quantified at 415.04 MPa for the rectangular profile, while registering slightly higher at 423.80 MPa for the I-profile configuration, depicting a discrepancy of 8.76 MPa, equivalent to approximately 2.07%. Notably, this discernible difference diminishes gradually towards the tip. For instance, at the position 6.75 m along the span, the rectangular profile yields a normal stress value of 46.95 MPa, whereas the I-profile counterpart records a slightly elevated reading of 49.82 MPa, resulting in a disparity of 2.87 MPa or approximately 5.76%.

The outcomes of the Finite Element Method (FEM) shear stress computations depicted in Figure 11 illustrate the distribution of shear stress across a spar, a critical structural component of a wing. Shear stress, defined as the force per unit area acting parallel to the surface of the spar, is visually represented using a color gradient within the image, transitioning from blue (indicating low stress) to red (indicating high stress). Moreover, numerical values corresponding to shear stress across various sections of the spar are provided. Notably, the image highlights that shear stress levels are notably elevated at the base where the spar interfaces with another component, implying substantial mechanical loading in this region.

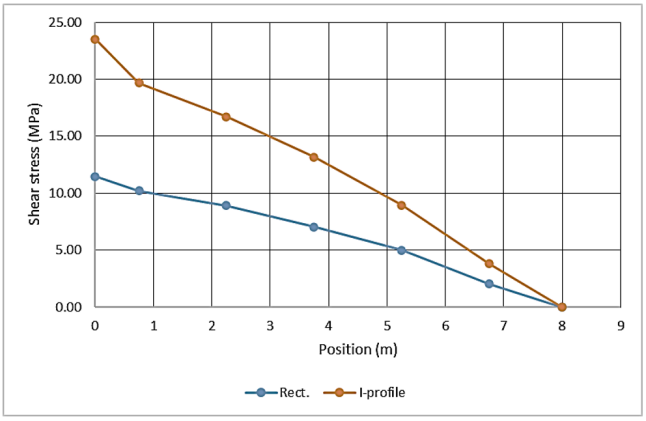


**Figure 12.** Shear Stress Comparison of Different Cross Section

Upon thorough scrutiny and comparison, as depicted in Figure 12, it becomes conspicuous that the shear stress values associated with both profiled spars exhibit discernible distinctions due to the identical web thickness. Notably, the cross-sectional area of the box profile web is twice that of the I-profile. The most notable dissimilarity, amounting to 12.04 MPa, manifests itself at the wing root position, with shear stress measuring 11.47 MPa for the rectangular profile and 23.51 MPa for the I-profile. This variance gradually diminishes towards the wingtip. Specifically, at position 6.75 m along the span, the shear stress is gauged at 2.02 MPa for the rectangular profile and 3.81 MPa for the I-shaped counterpart, resulting in a disparity of 1.79 MPa.

The maximum shear stress in both spar profiles remains significantly below the shear strength of Al7075-T6 material. Additionally, there's a disparity in mass, with the rectangular profile weighing 119.12 kg and the I-profile weighing 104.03 kg. Consequently, the selection of the I-profile merits consideration.

The comparison between normal stress and shear stress, conducted using mathematical analysis and FEM for a square profile, reveals distinct values as depicted in Figure 11. Normal stress, depicted by the black line, demonstrates that FEM values are generally lower than those obtained through mathematical analysis, albeit the variance is relatively small. The most significant deviation occurs at the spar base, measuring 6.40 MPa, gradually diminishing towards the wing's end to 1.7 MPa at position 6.75 m. In terms of shear stress, represented by the blue color, FEM values surpass those of mathematical analysis. At the root, the discrepancy is 1 MPa, fluctuating towards the tip and differing by 0.43 MPa at position 6.75 m.

The discrepancy between mathematical computations and FEM results for the I-profile (as depicted in Figure 14) follows a similar pattern to that observed in the square profile. Normal stress values (colored in black) calculated by FEM are 4.21 MPa lower than the mathematical values at the spar base, gradually reducing to 1.51 MPa at position 6.75 m in a linear manner. In terms of shear stress (illustrated in blue line), there is a difference of 2.57 MPa at the base and 0.63 MPa at position 6.75 m.

## 4. Conclusion

The success of a wing spar's design depends on its capacity to withstand applied loads without compromising structural integrity. This study focuses on the design and analysis of the wing-tip spar segment, extending from the mid-section to the wing's tip, specifically tailored for a Medium Altitude Long Endurance (MALE) UAV. It has been validated that the spar segment will not experience permanent deformation under a 4g load factor.

The greatest variance in normal stress levels between the rectangular and I-profiles amounts to 8.76 MPa, observed at the wing root location, while the most minimal divergence registers at 2.87 MPa, noted at the wing tip position at 6.75 m.

With respect to shear stress metrics, the widest disparity reaches 12.04 MPa, situated at the wing root, with the least contrast noted at 1.79 MPa, pinpointed at the wing tip position at 6.75 m.

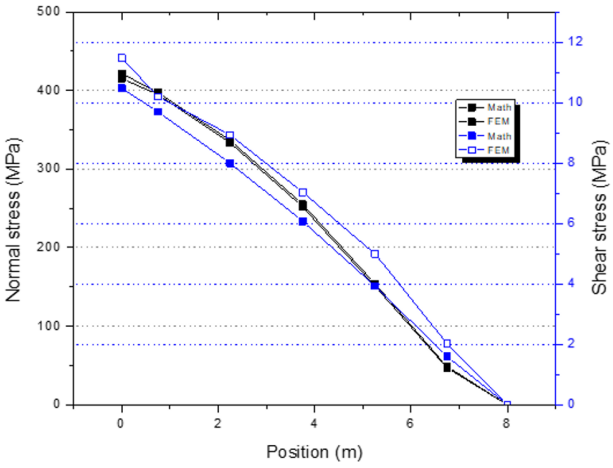


**Figure 13.** Math and FEM Stresses of Rectangular

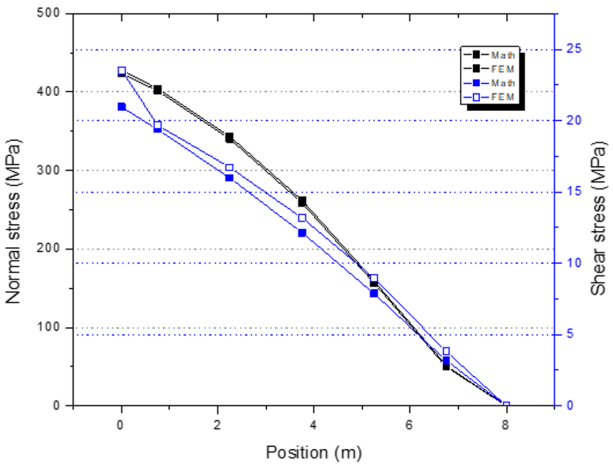


**Figure 14.** Math and FEM Stresses of I-Profile

Selecting the I-profile for the spar deserves consideration as it could lead to a weight reduction of 15 kg. Despite experiencing higher shear stress compared to the rectangular one, it remains significantly below its shear strength.

The comparison of normal stress of rectangular spar generally indicates lower FEM values compared to mathematical analysis, with the most significant deviation observed at the spar root (6.40 MPa decreasing to 1.7 MPa at 6.75 m), while FEM shear stress values exceed those of mathematical analysis, with a 1 MPa discrepancy at the root, fluctuating by 0.43 MPa at 6.75 m. Similarly, the discrepancy in the I-profile follows a similar trend, with FEM normal stress values lower by 4.21 MPa at the base, reducing to 1.51 MPa at 6.75 m, and shear stress differing by 2.57 MPa at the root and 0.63 MPa at 6.75 m.

## References


[1] O. H. Shaaban Ali, A. Gopalakrishnan, A. Muriyan, and S. Francis, "Unmanned aerial vehicles: A literature review," *Journal of Hunan University Natural Sciences*, vol. 49, no. 7, 2022.

[2] A. A. Laghari, A. K. Jumani, R. A. Laghari, and H. Nawaz, "Unmanned aerial vehicles: A review," *Cognitive Robotics*, vol. 3, pp. 8–22, 2023.

[3] F. Hasim, A. F. Widodo, *et al.*, "Analisa prestasi terbang dan kestabilan pesawat udara nir-awak (punabppt) prototipe sriti menggunakan cfd," in *Prosiding SIPTEKGAN XVI-2012 Seminar Nasional IPTEK Dirgantara XVI Tahun 2012*, pp. 341–351, Pusat Teknologi Penerbangan, 2012.

[4] F. R. Triputra, B. R. Trilaksono, R. A. Sasongko, and M. Dahsyat, "Longitudinal dynamic system modeling of a fixed-wing uav towards autonomous flight control system development: A case study of bppt wulung uav platform," in *2012 International Conference on System Engineering and Technology (ICSET)*, pp. 1–6, 2012.

[5] M. K. Sawant and A. G. Dahake, "A new hyperbolic shear deformation theory for analysis of thick beam," *International Journal of Innovative Research in Science, Engineering and Technology*, vol. 3, no. 2, pp. 9636–9643, 2014.

[6] O. U. P. J. O.A. Dada, O.M. Makinde, "A taguchi based iterative wing structural design for a low speed, hybrid uav," *Nigerian Journal of Technology*, vol. 41, p. 83–89, Mar. 2022.

[7] G. Visnjic, D. Nožak, F. Kosel, and T. Kosel, "Reducing shear-lag in thin-walled composite i-beam wing spars," *Aircraft Engineering and Aerospace Technology: An International Journal*, vol. 86, no. 2, pp. 89–98, 2014.

[8] C. E. D. S. M. L. Cassão Gatelli, L. Gomes and D. M. D. Leon, "A mdo process for preliminary design of a remotely piloted aircraft," in *Anais do X Congresso Nacional de Engenharia Mecânica*, 2018.

[9] B. N. B. Chinni and P. Siddappa, "Design and analysis of front spar wing-tip segment for a small transport aircraft," *Materials Today: Proceedings*, vol. 52, pp. 1846–1851, 2022.

[10] O. Schrenk, "A simple approximation method for obtaining the spanwise lift distribution," *The Aeronautical Journal*, vol. 45, no. 370, pp. 331–336, 1941.

[11] J. D. Fuentes, S. Cicero, F. Berto, A. R. Torabi, V. Madrazo, and P. Azizi, "Estimation of fracture loads in al7075-t651 notched specimens using the equivalent material concept combined with the strain energy density criterion and with the theory of critical distances," *Metals*, vol. 8, no. 2, p. 87, 2018.

[12] H.-S. A. P. M. Alloys, "Properties and selection: Nonferrous alloys and special-purpose materials," 1990.